Liu, L.; Lopez-Haro, M.; Meira, DM.; Concepción Heydorn, P.; Calvino, JJ.; Corma Canós, A. (2020). Regioselective Generation of Single-Site Iridium Atoms and Their Evolution into Stabilized Subnanometric Iridium Clusters in MWW Zeolite. Angewandte Chemie International Edition. 59(36):15695-15702. https://doi.org/10.1002/anie.202005621

# Regioselective Generation of Single-Site Ir Atoms and their Evolution into Stabilized Subnanometric Ir Clusters in MWW Zeolite

Lichen Liu,[1] Miguel Lopez-Haro,[2] Debora M. Meira,[3,4] Patricia Concepcion,[1] Jose J. Calvino[2] and Avelino Corma[1]*

[1] *Instituto de Tecnología Química, Universitat Politècnica de València-Consejo Superior de Investigaciones Científicas, Av. de los Naranjos s/n, Valencia 46022, Spain*

[2] *Departamento de Ciencia de los Materiales e Ingeniería Metalúrgica y Química Inorgánica, Facultad de Ciencias, Universidad de Cádiz, Cádiz, Spain*

[3] CLS@APS sector 20, Advanced Photon Source, Argonne National Laboratory, 9700 S. Cass Avenue, Argonne, IL 60439, USA

[4] Canadian Light Source Inc., 44 Innovation Boulevard, Saskatoon, Saskatchewan S7N 2V3, Canada

*Corresponding author. Email: acorma@itq.upv.es

## Abstract

Preparation of supported metal catalysts with uniform particle size and coordination environment is a challenging and important topic in materials chemistry and catalysis. In this work, we report the regioselective generation of single-site Ir atoms and their evolution into stabilized subnanometric Ir clusters in MWW zeolite, which are located at the 10MR window connecting the two neighboring 12MR supercages. The size of the subnanometric Ir clusters can be controlled by the post-synthesis treatments and maintain below 1 nm even after being reduced at 650 ºC, which cannot be readily achieved with samples prepared by conventional impregnation methods. The high structure sensitivity, size-dependence, of catalytic performance in the alkane hydrogenolysis reaction of Ir clusters in the subnanometric regime is evidenced.

## Introduction

One important direction in the preparation of heterogeneous metal catalysts is to generate well-defined single-site structures on solid carriers, in which the desired chemical composition and coordination environment of the metal sites are uniformly constructed.[1] If so, the electronic and geometric structures of metal sites will achieve homogeneity and those metal species should give high chemoselectivity in catalytic reactions, as the active centers in natural enzymes.[2] From a structural point of view, the active centers in heterogeneous single-site metal catalysts can be constructed by two components: the metal site containing one single atom or a combination of a group of atoms and the coordination environment from the support.[3,4] To achieve homogeneity in heterogeneous metal catalysts, the control of atomicity and the coordination environment of the metal species should be achieved simultaneously.

During the last decades, numerous methods have been developed for the generation of atomically dispersed metal catalysts on solid carriers.[5] Considering the electronic interaction between metal entities and the support and the steric effect from the solid carrier, the reactivity of each single metal atoms may also vary dramatically when the singly dispersed metal atoms locate in different sites on the support.[6] In recent years, most of the single-atom catalysts are generated on solid carriers such as metal oxides and heteroatom (N, P, S, etc)-doped carbons, in which the surface properties of those solid carriers are quite complicated and the location of metal atoms is usually randomly distributed. To achieve high homogeneity with the coordination environment of the metal atoms, a very low metal loading is required.[7]

In the case of supported metal catalysts made by subnanometric metal clusters, the preparation of well-defined catalysts with high uniformity can also be a challenge. It has been found that metal clusters with a few atoms can be generated in solution during the catalytic reaction, however, those metal clusters show a diverse size distribution and may further agglomerate into larger particles.[8,9] Using organometallic precursors, Gates et al. have shown the possibility to generate well-defined isolated metal atoms and metal clusters on various solid carriers.[10,11] But the presence of organic ligands may also block the metal clusters from reactants and the removal of the organic ligands can cause the decomposition of the ligands and sintering of metal clusters into nanoparticles.[12] Chaudret et al. have shown the transformation of the organometallic compounds by low-temperature reduction

treatments, resulting the formation of highly uniform small metal particles.[13,14]

To achieve uniform heterogeneous single-site metal catalysts, the utilization of a support with well-defined structure should be a precondition. In this context, zeolites can be an ideal choice due to its regular porous structures and high stability for potential practical applications.[15-18] Though there are still multiple possibilities to accommodate the metal atoms or clusters, it is possible to generate and stabilize single-site metal catalysts in specific position of zeolite structure, if a proper synthesis methodology can be developed to anchor those subnanometric metal entities in the desired position.[19]

In this work, we will report a one-pot synthesis approach to generate isolated Ir atoms in the 10R window connecting the neighboring 12R supercages in pure-silica MWW zeolites. Furthermore, after high-temperature reduction treatment by $H_2$, those isolated Ir atoms can form subnanometric Ir clusters (ca. 0.4-0.8 nm) at the 10R window between the supercages within MWW zeolite. In other words, by controlling the temperature of the reduction treatment, we can modulate the average size of Ir clusters in the subnanometric regime (ca. 0.4-0.8 nm), which cannot be readily achieved by conventional impregnation methods. We will also show the highly structure sensitive character, i.e. size dependence, of the alkane hydrogenolysis reaction on those subnanometric Ir clusters stabilized into MWW channels.

## Results and Discussions

By one-pot synthesis, subnanometric Ir species can be encapsulated in pure-silica MWW zeolite by adding the Ir precursor into the synthesis mixture for hydrothermal synthesis (see supplementary information for experimental details). As shown in **Figure S1**, the Ir@MWW sample presents the typical diffraction patterns of the purely siliceous MWW zeolite.[20] The typical sheet-like morphology of Ir@MWW material has also been confirmed by field-emission scanning electron microscopy (FESEM) (see **Figure S2**).

According to the structural features of MWW zeolite, there are several possible sites for the accommodation of isolated metal species, as described and discussed in **Figures S3-S5**. Herein, we have employed the newly developed STEM-iDPC (scanning transmission electron microscopy, integrated differential phase contrast) imaging technique to directly study size and position of Ir species encapsulated in MWW zeolite crystallites.[19,21,22] Firstly, we have studied the as synthesized

Ir@MWW-OSDA sample, which is obtained after the hydrothermal synthesis and still contains the organic structure-directing agent (OSDA). As can be seen in **Figure S6**, atomically dispersed Ir species with good dispersion can be observed in the high-resolution HAADF-STEM images. Taking into account the structure of MWW zeolite, there are several possible sites to accommodate isolated Ir atoms, as depicted in **Figures S3-S4**. By carefully correlating the paired HAADF-STEM and iDPC images, it can be concluded that, Ir atoms appear in several locations, including sites at the 10MR window between the 12MR supercages and in the 12MR supercages, as illustrated in **Figure S6**. This is consistent with a recent work on the identification of the location of the triad silanol species in SSZ-70, a related pure-silica zeolite to the MWW zeolite studied in this work.[23] In the as-synthesized Ir@MWW-OSDA sample, The Ir precursor is surrounded by the organic template molecules, encapsulated in the cages and cavities inside the MWW zeolite crystallites.

After calcination in air at 560 ºC for the removal of the organic structure-directing agent, a Ir@MWW-560air sample is obtained. As shown in **Figure 1 and Figure S7**, this sample also consists of atomically dispersed Ir species, indicating that the high-temperature calcination treatment does not cause the sintering of Ir atoms. Furthermore, on the basis of image simulation and experimental STEM-iDPC images, we have found that the isolated Ir atoms in the 0.24Ir@MWW-560air sample are regioselectively located in the 10MR window between the two supercages of MWW zeolite.[24,25]

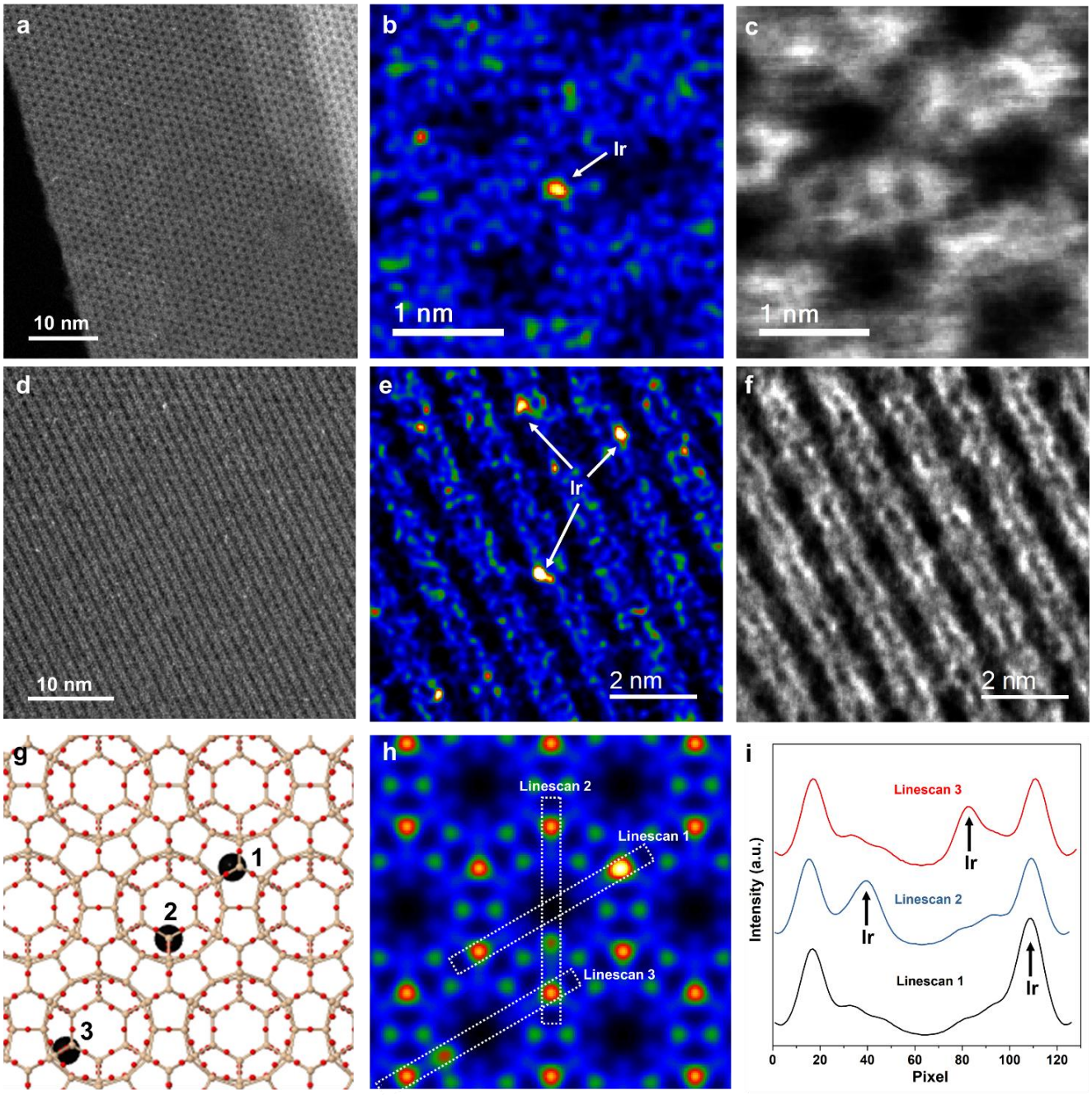


**Figure 1.** Structural characterization of Ir@MWW-560air sample. (a) Low-magnification HAADF-STEM image of Ir@MWW-560air sample along the [001] orientation, showing the presence of atomically dispersed Ir species in the MWW zeolite crystallite. The 12MR surface "cup" can also be visualized in this image. (b) High-resolution HAADF-STEM image and (c) the corresponding iDPC image of Ir@MWW-560air sample along the [001] orientation. In (b), a single Ir atom can be observed and its location can be determined to be at the 10MR window between the two neighboring 12MR supercages. (d) Low-magnification HAADF-STEM image of Ir@MWW-560air sample along the

tilted-[001] orientation, showing the presence of atomically dispersed Ir species in the MWW zeolite crystallite. (e) High-resolution HAADF-STEM image and (f) the corresponding iDPC image of Ir@MWW-560air sample along the tilted-[001] orientation. In (e), a single Ir atom can be observed and its location can be determined to be at the 10MR window between the two neighboring 12MR supercages. (g) Model of MWW zeolite with isolated Ir atoms located at different positions. Ir-1 atom is located at the 10MR window connecting the two neighboring 12MR supercages. Ir-2 atom is located within the 12MR supercage while the Ir-3 atom is located in the 10MR circular channel. (h) Simulated HAADF-STEM image of the model shown in (g) and the corresponding intensity profiles of the linescans indicated in (h). By correlating the experimental and simulated images, we can identify the location of isolated Ir atoms in the Ir@MWW-560air sample, which are at the 10MR window connecting the two neighboring 12MR supercages.

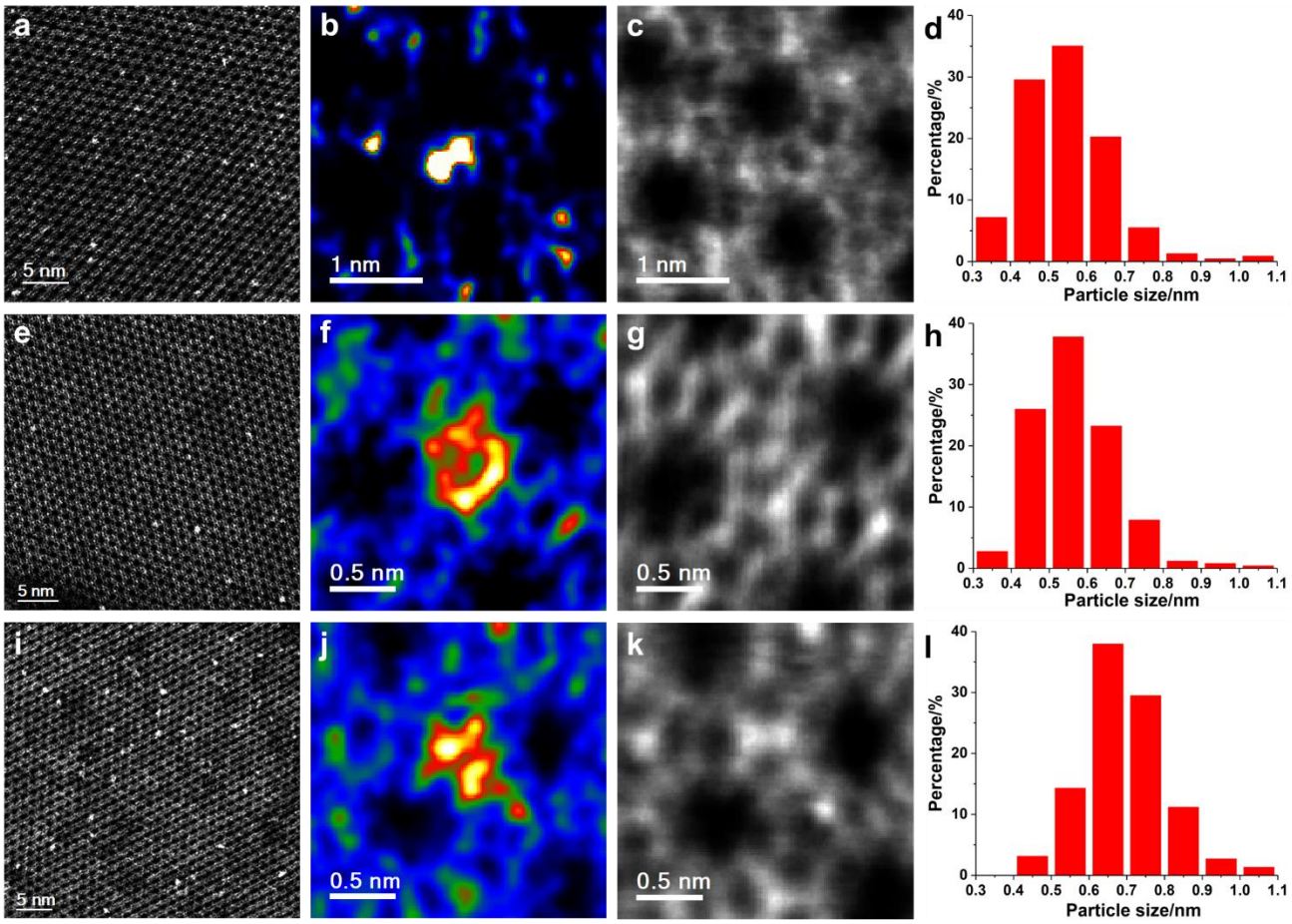


**Figure 2.** Structural characterization of Ir@MWW samples containing Ir clusters confined in MWW zeolite crystallites. (a-d) Ir@MWW-400$H_2$, (e-h) Ir Ir@MWW-500$H_2$ and (i-l) Ir@MWW-650$H_2$. For each sample, a low-magnification HAADF-STEM image is presented (a, e and i) to show the good

dispersion of subnanometric Ir clusters in the MWW zeolite crystallites. Furthermore, high-resolution HAADF-STEM images (b, f and j) and corresponding iDPC images (c, j and k) are presented to clarify the location of Ir clusters, which is determined to be at the 10MR window connecting the two neighboring 12MR supercages. The size distribution of Ir clusters in the three samples are also shown in (d, h and i).

It can be expected that, these isolated Ir atoms can evolve into Ir clusters after reduction by $H_2$, as previously observed with the Pt atoms located in the 10MR sinusoidal channels of MFI zeolite and with other Ir-zeolite materials in the literature.[26,27] Indeed, as shown in **Figure 2 and Figure S8-S9**, after reduction by $H_2$ at 400 ºC (named as 0.24Ir@MWW-400$H_2$), Ir clusters with good distribution in the zeolite crystallites are formed and the vast majority of the Ir clusters in this sample fall in the range of 0.3-0.7 nm. Notably, 70% of the total Ir particles are below 0.6 nm. These Ir clusters are located at the 10MR window between the two neighboring 12MR supercages as identified by the STEM-iDPC images and confirmed by the image simulation studies (see **Figures S10-S11**). It should be noted that, some isolated Ir atoms can still be observed in the HAADF-STEM images. When the reduction temperature is further increased up to 500 ºC (named as Ir@MWW-500$H_2$), the size distribution of Ir clusters remain almost unchanged, indicating the high stability of Ir species confined in the MWW (see **Figure S12-S14**). Even when the reduction temperature is further increased to 650 ºC (named as 0.24Ir@MWW-650$H_2$), the size distribution of Ir clusters only shows a slight increase in average size (see **Figures S15-S17**) and the fraction of Ir clusters below 0.6 nm decreases to ~40%. Nevertheless, the location of Ir clusters is also preserved after high-temperature reduction treatment, confirming the high stability of Ir clusters confined within the MWW zeolite structure. Nonetheless, after reduction by $H_2$ at 650 ºC, the fraction of Ir clusters above 0.7 nm in size clearly increases, indicating the decrease of smaller Ir clusters after the high-temperature reduction treatment.

The size evolution of Ir species confined in MWW zeolite crystallites is also reflected in the characterization results by X-ray absorption spectroscopy (XAS). For the starting Ir@MWW-560air sample, from the X-ray absorption near edge structure (XANES) results we can observe that the edge position is the same from the $IrO_2$ reference. In addition, the higher white line intensity indicates the higher density of unoccupied states in agreement with the mononuclear Ir(IV) species. From the

extended X-ray absorption fine structure spectroscopy (EXAFS) results, we can observe a Ir-O contribution as well as a Ir-Si contribution reflecting the Ir high dispersion and interaction with the support (see **Table 1**).[28] The Ir-O contribution may come from the interaction of Ir atoms with both framework oxygen and extra-framework oxygen. After being in situ reduced by $H_2$ at 400 ºC, the isolated Ir(IV) species in the starting material become partially reduced, as can be seen in the decrease of white line intensity in XANES spectrum (see **Figure 3a**) and the decrease of Ir-O contribution (at ~2.0 Å) in EXAFS spectrum (see **Figure 3b**). The appearance of a metallic Ir-Ir contribution (at ~2.7 Å) is also consistent with the observation of Ir clusters in the HAADF-STEM images. The coordination number of first-shell Ir-Ir contribution is around 6 according to the fit results and the uncertainty of the analysis results caused by the low Ir loading in the Ir@MWW samples (see **Table 1**). A similar coordination number for the first-shell Ir-Ir contribution is obtained for the reduced Ir@MWW samples at 400-650 ºC, indicating the high stability of confined Ir clusters. The fit results of the EXAFS spectra suggest that the average size of the Ir particles in the three reduced Ir@MWW samples is ~0.9 nm. Considering the presence of a small fraction of metallic Ir nanoparticles (>2 nm) on the external surface of MWW zeolite crystallites formed by the reduction of $IrO_2$ nanoparticles, we can conclude that the majority of Ir particles should exist as subnanometric Ir clusters, which is consistent with the electron microscopy images.[29,30]

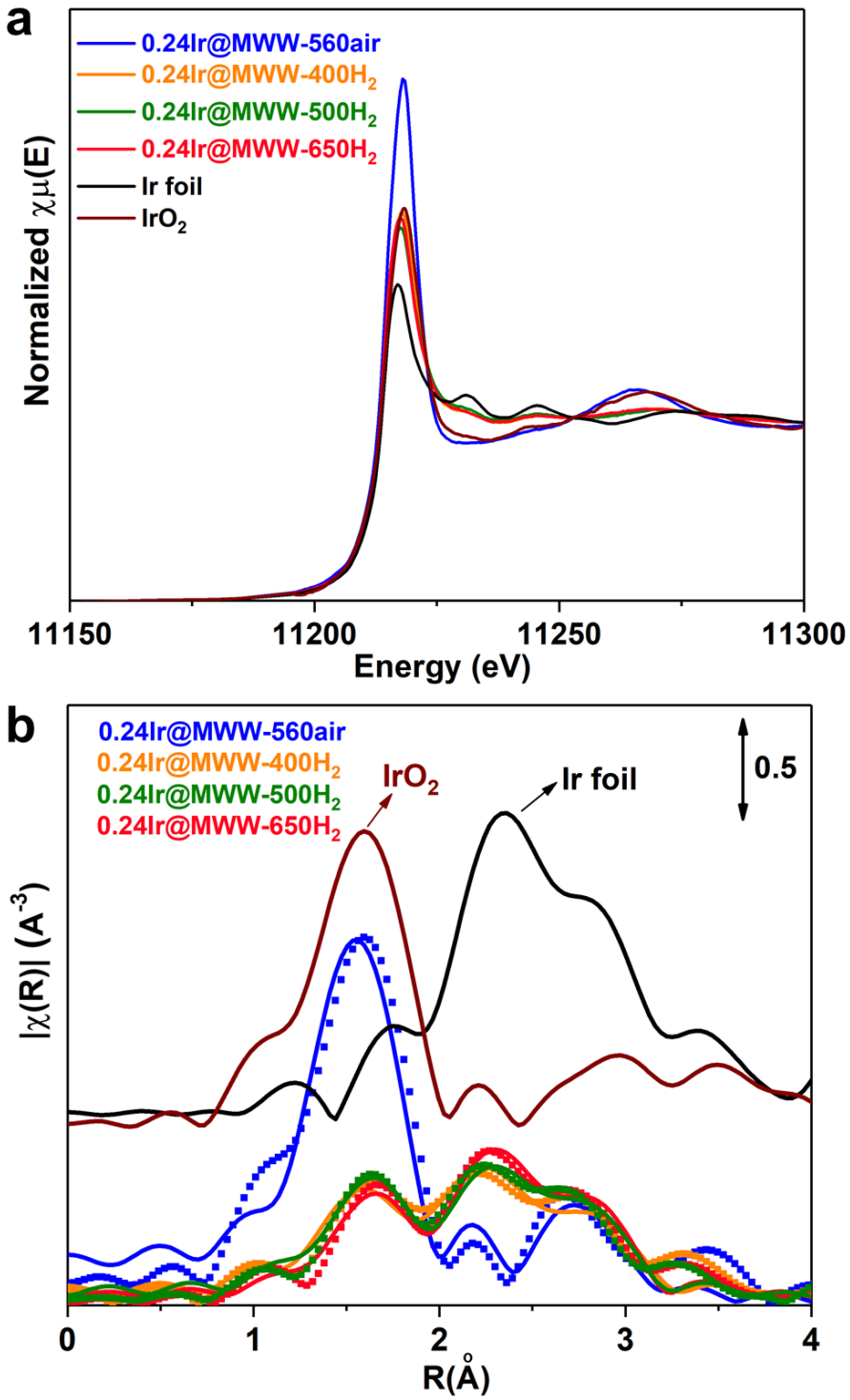


**Figure 3.** Characterization of 0.24Ir@MWW samples by in situ XAS. (a) XANES and (b) EXAFS spectra of 0.24Ir@MWW samples after different treatments. The 0.24Ir@MWW-560air sample was measured directly while the other reduced 0.24Ir@MWW samples were reduced at given temperature by $H_2$ and then cooled to room temperature before the collection of the spectra.

**Table 1.** Fit results of the EXAFS results of 0.24Ir@MWW samples prepared by one-pot synthesis.

| | Ir(IV) phase | | | | | Metallic Ir phase | | | R-factor |
|---|---|---|---|---|---|---|---|---|---|
| Sample | CN (Ir-O) | R (Å) | CN (Ir-Si) | R (Å) | $\sigma_i^2$ (Å$^2$)* | CN (Ir-Ir) | R (Å) | $\sigma_i^2$ (Å$^2$)* | |
| 0.24Ir@MWW-560air | 6±1 | 1.97± 0.01 | 3±1 | 3.27± 0.03 | 0.003± 0.002 | | | | 0.027 |
| 0.24Ir@MWW-400H$_2$ | 3±1 | 1.98± 0.02 | | | 0.008± 0.007 | 6±2 | 2.70 ± 0.01 | 0.004 ±0.003 | 0.017 |
| 0.24Ir@MWW-500H$_2$ | 1.4±0.6 | 1.96± 0.02 | | | 0.003± 0.006 | 7±2 | 2.70 ± 0.01 | 0.004 ±0.002 | 0.015 |
| 0.24Ir@MWW-650H$_2$ | 2.3±0.8 | 1.98± 0.02 | | | 0.006± 0.005 | 6±2 | 2.70 ± 0.01 | 0.003 ±0.002 | 0.016 |

CN, coordination number; R, bonding length; $\sigma_i^2$, Debye-Waller factor. The 0.24Ir@MWW-560air sample was measured directly at room temperature without any pre-treatments. The reduced 0.24Ir@MWW samples were reduced by $H_2$ at given temperature and then cooled to room temperature in $H_2$ flow, before the acqusition of XAS spectra. * $\sigma_i^2$ for Ir-Si path was fixed to 0.003; ** R-factor measures the misfit between the data and the proposed model

Notably, a small portion of an Ir-O contribution can still be observed in the reduced Ir@MWW samples, regardless of the reduction temperature. The Ir-O contribution observed in EXAFS spectra can be associated to the presence of isolated Ir atoms by high-resolution HAADF-STEM images in the reduced Ir@MWW samples (see **Figure S11** and **S14**) and the bonding between the Ir clusters and the zeolite framework (probably in the form of $Ir_n$-O-Si bonding).[31] However, considering the EXAFS fit results (see additional discussion in **supporting information**) and the analysis of a large number of HAADF-STEM images, the amount of isolated Ir atoms in the three reduced Ir@MWW samples should be below 10%, especially in the case of the 0.24Ir@MWW-650$H_2$ sample.

For comparison, two Ir/MWW samples were prepared by conventional incipient wetness impregnation. The Ir loading was controlled to be 0.07 wt% and 0.25 wt%, respectively. For the 0.07Ir/MWW-imp samples, the pre-reduction activation conditions have a significant influence on the particle size. Ir clusters mainly of 0.4~0.9 nm are formed after reduction at 400 ºC and the size grows to 0.6-1.2 nm after reduction by $H_2$ at higher temperature (500 and 650 ºC) (see **Figures S18-20**). By comparing the Ir particles in the 0.07Ir/MWW-imp samples with the 0.24Ir@MWW samples, larger

average particle sizes and broader size distributions (see **Figure S21**) can be found with the impregnated 0.07Ir/MWW-imp samples, though the Ir loading is much lower. Moreover, the location of Ir particles in the 0.07Ir/MWW-imp-650$H_2$ sample has been studied by STEM-iDPC and some Ir particles (~1 nm) have been found in the surface "cups" of the MWW zeolite crystallites (see **Figure S22**), because this sample was prepared by conventional wetness impregnation, as described in **Figure S23**.

In the case of Ir/MWW-imp sample with 0.25 wt% of Ir (similar Ir loading as the 0.24Ir@MWW sample prepared by one-pot synthesis), a mixture of Ir nanoparticles and Ir clusters are formed in the 0.25Ir/MWW-imp sample after being reduced by $H_2$ at 400 $^oC$ (see **Figure S24**). Increasing the reduction temperature to 500 and 650 $^oC$ causes further sintering of Ir clusters into Ir nanoparticles (see **Figures S25-S26**). We have also studied the influence of Ir loading on the particle size for the Ir@MWW sample prepared by one-pot synthesis. As shown in **Figure S27**, the good dispersion of subnanometric Ir clusters in the MWW zeolite crystallites is maintained even when the Ir loading is increased to ~0.5 wt% (named as 0.5Ir@MWW-400$H_2$). Moreover, the Ir clusters in this sample are also mainly located at the 10MR windows connecting the two neighboring supercages (see **Figure S28**). The good dispersion of subnanometric Ir clusters in the 0.5Ir@MWW-400$H_2$ sample has also been confirmed by EXAFS, which gives a first-shell Ir-Ir coordination number of ~7, corresponding to an average size of ~1 nm (see **Figure S29** and **Table S1**). Though the coordination number increases slightly as compared to the 0.24Ir@MWW-400$H_2$ sample, the majority of the Ir species in this sample should exist as subnanometric Ir clusters, as can be seen in the HAADF-STEM images. These results indicate that the one-pot synthesis method is an effective strategy to encapsulate subnanometric Ir clusters into the MWW zeolite structure with high regioselectivity and stability against sintering.

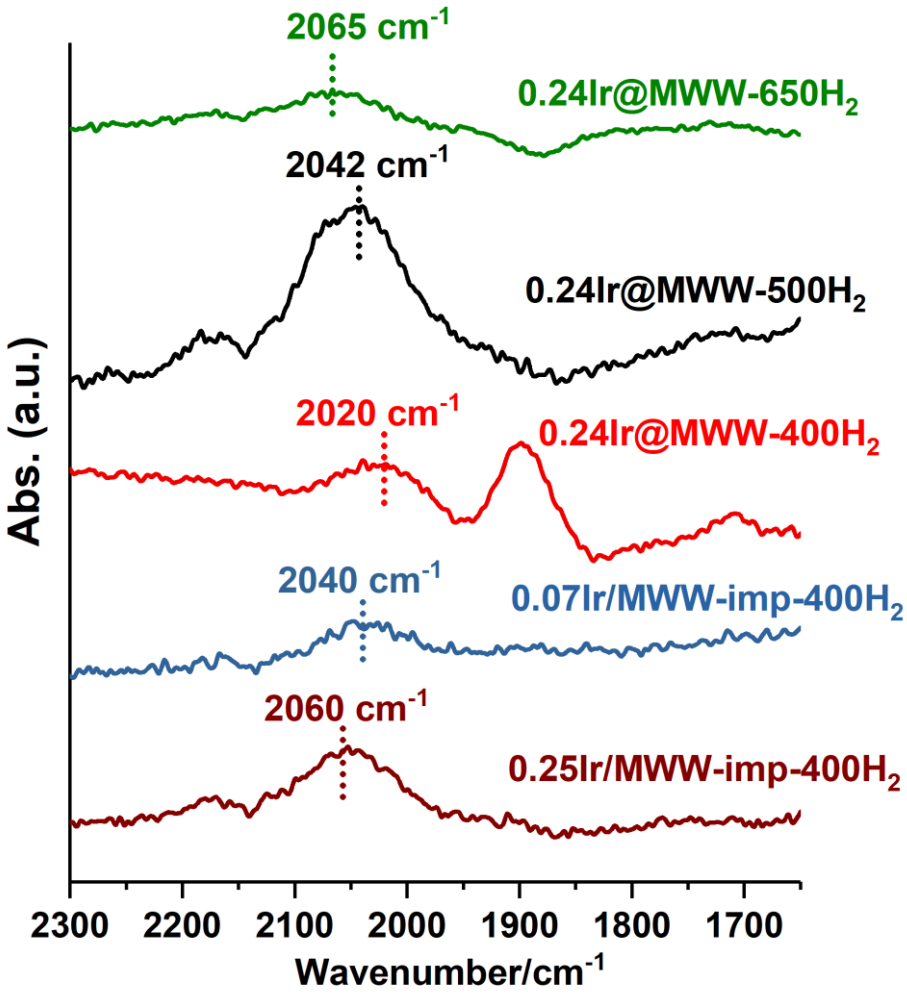


**Figure 4.** CO-IR spectra of Ir@MWW samples prepared by one-pot synthesis and Ir/MWW-imp sample prepared by conventional impregnation. All the samples have been reduced in $H_2$ at a given temperature and then dosed with CO at room temperature before collecting the IR spectra.

To obtain more information on the influence of reduction treatment on the structure of Ir clusters confined in MWW zeolite, we have measured the IR spectra of various Ir-MWW samples using CO as probe molecules. The position of the terminal CO adsorption band is sensitive to the electronic properties of the Ir species, which is also associated to the particle size.[32] As displayed in **Figure 4**, a clear shift of the terminal CO adsorption band on Ir clusters from 2020 to 2065 $cm^{-1}$ takes place when the reduction temperature increases from 400 to 650 ºC. This shift corresponds to an increase of the size of the clusters, which is consistent with the electron microscopy characterization results.[33] The CO adsorption band at ~1900 $cm^{-1}$ can be associated to bridged CO adsorbed on very small Ir clusters present in the 0.24Ir@MWW-400$H_2$ sample.[34] On the other hand, the variation of the size distribution

of the confined Ir clusters in the 0.24Ir@MWW samples is not as significant as the shift of the IR bands. One possible reason could be due to the change of the geometric structures of Ir clusters when being reduced at different temperatures.[35,36] Notably, the 0.07Ir/MWW-imp-400$H_2$ sample shows IR features similar to those of the 0.24Ir@MWW-500$H_2$ sample, though the size distribution of Ir clusters in this sample is closer to the 0.24Ir@MWW-650$H_2$ sample. Meanwhile, the 0.25Ir/MWW-imp-400$H_2$ sample shows similar IR features as the 0.24Ir@MWW-650$H_2$ sample. The spatial distribution of Ir clusters and the Ir-zeolite interaction are different for samples prepared by impregnation and one-pot synthesis. As a result, the interaction between the Ir clusters and CO probe molecules is also influenced, which is reflected in the shift of CO adsorption bands. Combining the characterization results from both electron microscopic and spectroscopic techniques, it can be concluded that, it is possible to modulate the size of subnanometric Ir clusters confined in MWW zeolites and the confinement effect from the zeolite framework on Ir clusters can be reflected on the interaction between Ir clusters and substrate molecules.

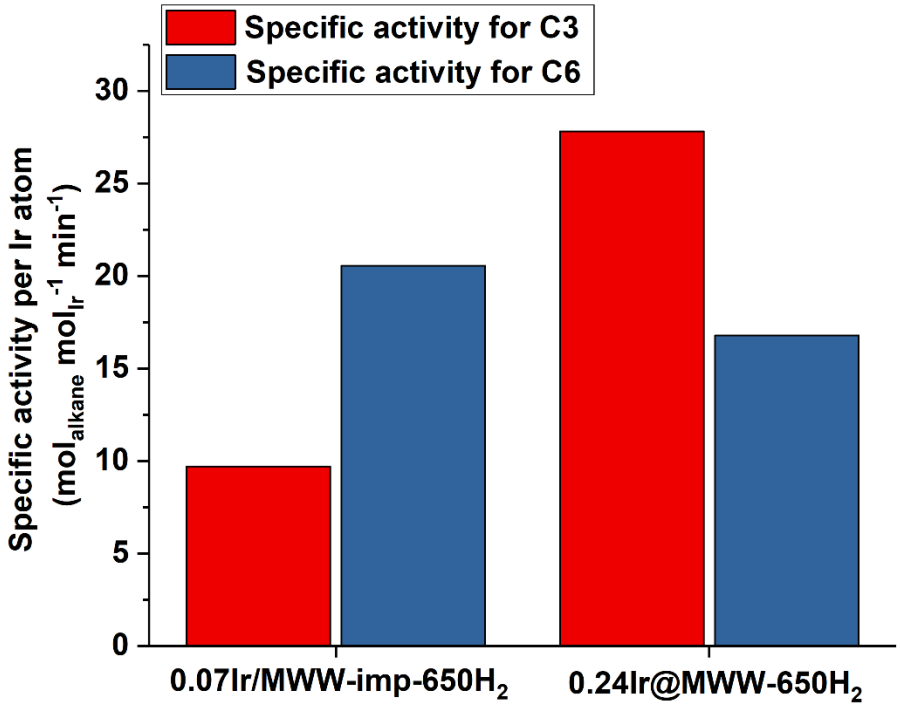


**Figure 5.** Comparison of the activity for hydrogenolysis of propane and n-hexane with 0.07Ir/MWW-imp-650$H_2$ and 0.24Ir@MWW-650$H_2$. The reaction was performed in a fix-bed reactor. The hydrogenolysis of propane was performed at 365 ºC while hydrogenolysis of n-hexane was performed at 350 ºC. Before the hydrogenolysis reaction, the catalyst was activated by reduction with $H_2$ at the

given temperature for 1 h and then cooled down to the reaction temperature in $H_2$ flow. Reaction conditions: 50 mg solid catalysts and a mixture of $H_2$ and propane ($H_2$/propane=24.5) as feed gas for all the catalytic tests. The reactivity shown in this figure was calculated based on three consecutive measures by on-line gas chromatography and the error is within ±3%. The conversion of propane was controlled to below 20%.

Supported Ir catalysts have been reported for hydrogenolysis reactions, which is used to open the cycloalkane rings or to decrease the chain length of alkanes. Herein, by using two alkane molecules with different chain length (propane and n-hexane) as probe reactants, we have compared the reactivity of 0.07Ir/MWW-imp-650$H_2$ and 0.24Ir@MWW-650$H_2$ for hydrogenolysis of alkanes to figure out the spatial distribution of Ir clusters generated by different methods. As shown in **Figure 5**, 0.07Ir/MWW-imp-650$H_2$ sample, comprising Ir particles mainly located on the external surface, exhibits higher specific activity for hydrogenolysis of n-hexane than propane, which is caused by the intrinsic high, as reported with Ir catalyst supported on silica.[37] Interestingly, the 0.24Ir@MWW-650$H_2$ sample exhibits higher specific activity for hydrogenolysis of propane than n-hexane. Since the diffusion of n-hexane across the 12MR supercages through the 10MR windows will be more difficult than propane, the lower reactivity of 0.24Ir@MWW-650$H_2$ sample for the larger reactant should be caused by the location of Ir clusters and the resultant low diffusion efficiency of n-hexane to the Ir clusters.[38] These results indicate that the majority of the Ir species in the 0.24Ir@MWW-650$H_2$ sample should be encapsulated inside the MWW zeolite crystallites, instead of being located on the external surface.

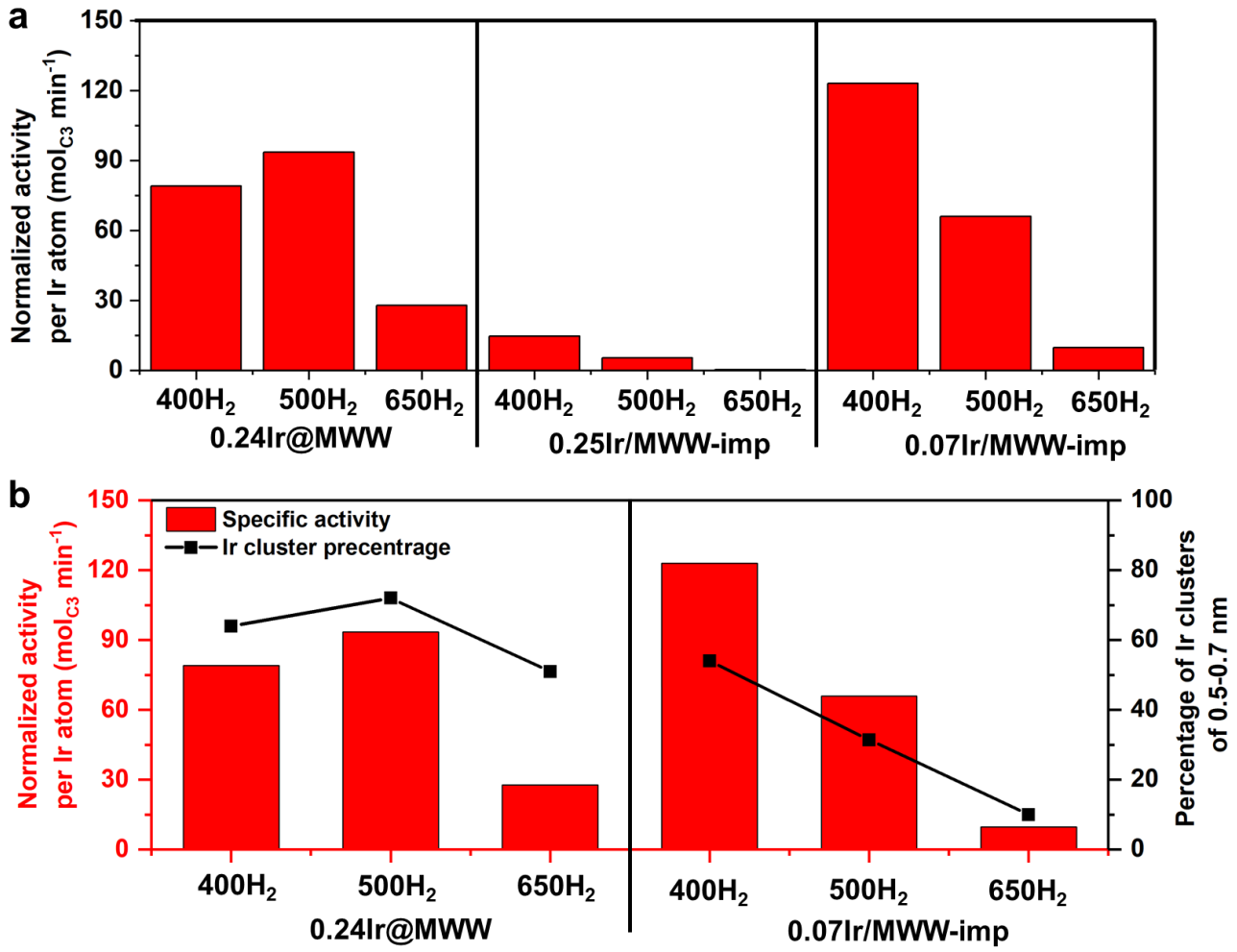


**Figure 6.** (a) Activity for hydrogenolysis of propane with different Ir-MWW catalysts. The reaction was performed at 365 °C in a fix-bed reactor. Before the hydrogenolysis reaction, the catalyst was activated by reduction with $H_2$ at the given temperature for 1 h and then cooled down to the reaction temperature in $H_2$ flow. Reaction conditions: 50 mg solid catalysts and a mixture of $H_2$ and propane ($H_2$/propane=24.5) as feed gas for all the catalytic tests. The reactivity shown in this figure was calculated based on three consecutive measures by on-line gas chromatography and the error is within ±3%. The conversion of propane was controlled to below 20%. (b) Correlation between the specific activity for hydrogenolysis of propane and the percentage of Ir clusters of 0.5-0.7 nm for various Ir-MWW zeolite catalysts.

It has been shown in the literature that, the hydrogenolysis of propane is a structure-sensitive reaction, which is related to the size and the geometric structure of Ir particles.[39,40] Those works were carried out with Ir particles supported on open-structure supports, i.e. silica and alumina.[41] On the

basis of the above structural characterization results, the Ir@MWW samples prepared by one-pot synthesis allow us to study the structure-reactivity correlation for alkane hydrogenolysis reaction at the subnanometric regime. As shown in **Figure 6a**, the two Ir-MWW samples with similar Ir loading, but prepared by different methods, show dramatically different reactivity for propane hydrogenolysis reaction under the same reaction conditions. When the Ir-MWW catalysts were activated by reduction with $H_2$ at 400 ºC, the 0.24Ir@MWW-400$H_2$ sample is 5 times more active than the 0.25Ir/MWW-imp-500$H_2$ sample. Notably, after being activated at 500 ºC, the 0.24Ir@MWW-500$H_2$ sample shows an enhanced activity with respect to 0.24Ir@MWW-400$H_2$, and which is up to ~17 times higher than that of the 0.25Ir/MWW-imp-500$H_2$ sample. The advantage of 0.24Ir@MWW sample over 0.25Ir/MWW-imp sample is even more significant (nearly two-orders of magnitude higher) when the activation by $H_2$ reduction treatment is performed at 650 ºC.

According to the whole set of structural characterization results described above, the size of the Ir particles in the 0.24Ir@MWW sample is much smaller than that in the 0.25Ir/MWW sample, implying that smaller Ir clusters are much more active than the Ir nanoparticles for hydrogenolysis of propane. Indeed, as can be seen in **Figure 6a**, the 0.07Ir/MWW-imp samples with smaller Ir particles show clearly much higher specific activity than the 0.25Ir/MWW samples under the same activation conditions. Moreover, when activated at 400 ºC, the 0.07Ir/MWW-imp-400$H_2$ sample containing Ir species on the external surface of MWW zeolite crystallites exhibits even higher activity than the 0.24Ir@MWW-400$H_2$ sample, which could be caused by either the size of Ir or the difficulty to reach all the encapsulated Ir clusters within the Ir@MWW sample, since Ir clusters are located in the 10MR windows between the two neighboring 12MR supercages. However, activity decreases significantly when the 0.07Ir/MWW-imp catalyst is pre-reduced at 500 ºC, while an enhancement is observed with the 0.24Ir@MWW-500$H_2$ sample after the same activation treatment. Even a more dramatic change is found with the 0.07Ir/MWW-imp sample after reduction at 650 ºC, which leads to a specific activity in the 0.24Ir@MWW-650$H_2$ sample roughly ~1/3 of that observed in the catalyst reduced at 400ºC. Though all the three samples show declined activity when increasing the activation temperature to 650 ºC, the activity decay with the 0.24Ir@MWW sample is much less than that observed in the samples prepared by impregnation, which could be associated with the higher stability of Ir clusters confined inside the MWW zeolite crystallites.

By correlating the structural characterization results (size distribution of Ir clusters and CO-IR) and the catalytic performance for propane hydrogenolysis reaction, we can deduce that the Ir clusters with CO adsorption band at ~2040 $cm^{-1}$ are the most active species, as observed with the 0.24Ir@MWW-500$H_2$ and 0.07Ir/MWW-imp-400$H_2$ sample. With larger Ir clusters, the activity is lower, especially when the particle size is increased above 1 nm. Since the 0.24Ir@MWW-500$H_2$ sample is more active than the 0.24Ir@MWW-400$H_2$ sample, there could be an optimized size of Ir clusters for the propane hydrogenolysis reaction. As shown in **Figure 6b**, we attempted to correlate the percentage of Ir clusters of around 0.6 nm (i.e. 0.5-0.7 nm) with the specific activity of various Ir catalysts. When comparing the 0.07Ir/MWW-imp samples prepared by conventional impregnation, a very good correlation is observed since higher percentage of Ir clusters of 0.5-0.7 nm leads to higher specific activity. In the case of 0.24Ir@MWW samples, the specific activity has also a positive correlation with the population of Ir clusters of 0.5-0.7 nm, though the relationship is not as linear as observed with the 0.07Ir/MWW-imp samples. As mentioned before, the difficulty of reactant diffusion to Ir clusters confined at the 10MR winding connecting the two neighboring 12MR supercages can cause the lower reactivity of the 0.24Ir@MWW sample, though a high percentage of Ir clusters of 0.5-0.7 nm is present.[42,43] Such influence can be more predominant in the case of 0.24Ir@MWW-650$H_2$ sample, in which the size of the Ir clusters match very well with the size of the 10MR windows between the 12MR supercages. Nevertheless, the higher activity of Ir clusters in the 0.24Ir@MWW-500$H_2$ sample than the Ir species in the 0.07Ir/MWW-imp-500$H_2$ indicates the size effect can compensate the diffusion limitation from the zeolite framework. The structure-reactivity relationship demonstrated in this work can be complementary to the results in the literature, which were obtained with supported Ir nanoparticles, indicating the unique catalytic behavior of subnanometric metal entities.[44,45] Nevertheless, our results also indicate the significant impacts of confinement effect on the structures and catalytic behavior of metal clusters.

## Conclusion

In summary, we have shown the regioselective generation of isolated Ir atoms at the 10MR window at the two neighboring 12MR supercages in MWW zeolite and the controllable formation of subnanometric Ir clusters at the same position. We have also found that, Ir clusters below 0.7 nm are

the optimized size for hydrogenolysis of propane. The synthesis and characterization methods developed in this work can also be extended for other metals for generation of subnanometric metal entities in MWW zeolite structure in specific location and used for activation of light alkanes.

## Acknowledgements

This work has been supported by the European Union through the European Research Council (grant ERC-AdG-2014-671093, SynCatMatch) and the Spanish government through the "Severo Ochoa Program" (SEV-2016-0683). The authors also thank Microscopy Service of UPV for the TEM and STEM measurements. High-resolution STEM measurements were performed at the DME-UCA node of the ELECMI National Singular Infrastruture, in Cadiz University, with financial support from FEDER/MINECO (MAT2017-87579-R and MAT2016-81118-P). This research used resources of the Advanced Photon Source, an Office of Science User Facility operated for the U.S. Department of Energy (DOE) Office of Science by Argonne National Laboratory, and was supported by the U.S. DOE under Contract No. DE-AC02-06CH11357, and the Canadian Light Source and its funding partners. The financial support from ExxonMobil on this project is also greatly acknowledged.

## References

[1] L. Liu, A. Corma, *Chem. Rev.* **2018**, *118*, 4981-5079.
[2] J. M. Thomas, R. Raja, D. W. Lewis, *Angew. Chem. Int. Ed.* **2005**, *44*, 6456-6482.
[3] A. Wang, J. Li, T. Zhang, *Nat. Rev. Chem.* **2018**, *2*, 65-81.
[4] J. D. Pelletier, J. M. Basset, *Acc. Chem. Res.* **2016**, *49*, 664-677.
[5] Y. Pan, C. Zhang, Z. Liu, C. Chen, Y. Li, *Matter* **2020**, *2*, 78-110.
[6] B. C. Gates, M. Flytzani-Stephanopoulos, D. A. Dixon, A. Katz, *Catal. Sci. Technol.* **2017**, *7*, 4259-4275.
[7] A. S. Hoffman, L. M. Debefve, S. Zhang, J. E. Perez-Aguilar, E. T. Conley, K. R. Justl, I. Arslan, D. A. Dixon, B. C. Gates, *ACS Catal.* **2018**, *8*, 3489-3498.
[8] J. Oliver-Meseguer, J. R. Cabrero-Antonino, I. Dominguez, A. Leyva-Perez, A. Corma, *Science* **2012**, *338*, 1452-1455.
[9] A. Corma, P. Concepcion, M. Boronat, M. J. Sabater, J. Navas, M. J. Yacaman, E. Larios, A. Posadas, M. A. Lopez-Quintela, D. Buceta, E. Mendoza, G. Guilera, A. Mayoral, *Nat. Chem.* **2013**, *5*, 775-781.
[10] P. Serna, B. C. Gates, *Acc. Chem. Res.* **2014**, *47*, 2612-2620.
[11] J. Lu, C. Aydin, N. D. Browning, B. C. Gates, *Angew. Chem. Int. Ed.* **2012**, *51*, 5842-5846.
[12] L. Liu, A. Corma, *Trends Chem.* **2020**, *2*, 383-400.
[13] C. Pan, K. Pelzer, K. Philippot, B. Chaudret, F. Dassenoy, P. Lecante, M. J. Casanove, *J. Am.*

*Chem. Soc.* **2001**, *123*, 7584-7593.
[14] L. M. Martinez-Prieto, B. Chaudret, *Acc. Chem. Res.* **2018**, *51*, 376-384.
[15] L. Liu, U. Diaz, R. Arenal, G. Agostini, P. Concepcion, A. Corma, *Nat. Mater.* **2017**, *16*, 132-138.
[16] Q. Sun, N. Wang, T. Zhang, R. Bai, A. Mayoral, P. Zhang, Q. Zhang, O. Terasaki, J. Yu, *Angew. Chem. Int. Ed.* **2019**, *58*, 18570-18576.
[17] Y. Liu, Z. Li, Q. Yu, Y. Chen, Z. Chai, G. Zhao, S. Liu, W. C. Cheong, Y. Pan, Q. Zhang, L. Gu, L. Zheng, Y. Wang, Y. Lu, D. Wang, C. Chen, Q. Peng, Y. Liu, L. Liu, J. Chen, Y. Li, *J. Am. Chem. Soc.* **2019**, *141*, 9305-9311.
[18] S. M. Wu, X. Y. Yang, C. Janiak, *Angew. Chem. Int. Ed.* **2019**, *131*, 12468-12482.
[19] L. Liu, M. Lopez-Haro, C. W. Lopes, C. Li, P. Concepcion, L. Simonelli, J. J. Calvino, A. Corma, *Nat. Mater.* **2019**, *18*, 866-873.
[20] M. A. Camblor, A. Corma, M.-J. Díaz-Cabañas, C. Baerlocher, *J. Phys. Chem. B* **1998**, *102*, 44-51.
[21] E. Yucelen, I. Lazic, E. G. T. Bosch, *Sci. Rep.* **2018**, *8*, 2676.
[22] L. Liu, N. Wang, C. Zhu, X. Liu, Y. Zhu, P. Guo, L. Alfilfil, X. Dong, D. Zhang, Y. Han, *Angew. Chem. Int. Ed.* **2020**, *59*, 819-825.
[23] C. Schroeder, C. Muck-Lichtenfeld, L. Xu, N. A. Grosso-Giordano, A. Okrut, C. Y. Chen, S. I. Zones, A. Katz, M. R. Hansen, H. Koller, *Angew. Chem. Int. Ed.* **2020**, doi: 10.1002/anie.202001364.
[24] A. Corma, V. Fornes, S. B. Pergher, T. L. M. Maesen, J. G. Buglass, *Nature* **1998**, *396*, 353-356.
[25] M. E. Leonowicz, J. A. Lawton, S. L. Lawton, M. K. Rubin, *Science* **1994**, *264*, 1910-1913.
[26] M. Moliner, J. E. Gabay, C. E. Kliewer, R. T. Carr, J. Guzman, G. L. Casty, P. Serna, A. Corma, *J. Am. Chem. Soc.* **2016**, *138*, 15743-15750.
[27] L. Liu, D. N. Zakharov, R. Arenal, P. Concepcion, E. A. Stach, A. Corma, *Nat. Commun.* **2018**, *9*, 574.
[28] W. Yan, S. Xi, Y. Du, M. K. Schreyer, S. X. Tan, Y. Liu, A. Borgna, *ChemCatChem* **2018**, *10*, 3078-3085.
[29] J. de Graaf, A. J. van Dillen, K. P. de Jong, D. C. Koningsberger, *J. Catal.* **2001**, *203*, 307-321.
[30] A. Jentys, *Phys. Chem. Chem. Phys.* **1999**, *1*, 4059-4063.
[31] J. Lu, P. Serna, C. Aydin, N. D. Browning, B. C. Gates, *J. Am. Chem. Soc.* **2011**, *133*, 16186-16195.
[32] A. Zhao, B. C. Gates, *J. Am. Chem. Soc.* **1996**, *118*, 2458-2469.
[33] H. Noei, D. Franz, M. Creutzburg, P. Müller, K. Krausert, E. Grånäs, R. Taube, F. Mittendorfer, A. Stierle, *J. Phys. Chem. C* **2018**, *122*, 4281-4289.
[34] A. Fielicke, P. Gruene, G. Meijer, D. M. Rayner, *Surface Science* **2009**, *603*, 1427-1433.
[35] T. R. Henninen, M. Bon, F. Wang, D. Passerone, R. Erni, *Angew. Chem. Int. Ed.* **2020**, *59*, 839-845.
[36] M. Okumura, Y. Irie, Y. Kitagawa, T. Fujitani, Y. Maeda, T. Kasai, K. Yamaguchi, *Catal. Today* **2006**, *111*, 311-315.
[37] D. W. Flaherty, E. Iglesia, *J. Am. Chem. Soc.* **2013**, *135*, 18586-18599.
[38] O. Talu, M. S. Sun, D. B. Shah, *AIChE Journal* **1998**, *44*, 681-694.
[39] D. W. Flaherty, A. Uzun, E. Iglesia, *J. Phys. Chem. C* **2015**, *119*, 2597-2613.
[40] D. D. Hibbitts, D. W. Flaherty, E. Iglesia, *ACS Catal.* **2015**, *6*, 469-482.
[41] A. Majesté, S. Balcon, M. Guérin, C. Kappenstein, Z. Paál, *J. Catal.* **1999**, *187*, 486-492.
[42] A. Corma, C. R. A. Catlow, G. Sastre, *J. Phys. Chem. B* **1998**, *102*, 7085-7090.

[43] G. Sastre, C. R. A. Catlow, A. Corma, *J. Phys. Chem. B* **2002**, *106*, 956-962.
[44] H. Shi, O. Y. Gutiérrez, G. L. Haller, D. Mei, R. Rousseau, J. A. Lercher, *J. Catal.* **2013**, *297*, 70-78.
[45] D. W. Flaherty, A. Uzun, E. Iglesia, *J. Phys. Chem. C* **2015**, *119*, 2597-2613.

# Table of Content

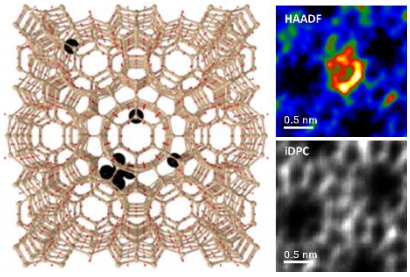


Isolated Ir atoms and subnanometric Ir clusters are regioselectively generated and stabilized in the 10MR window of MWW zeolite for shape-selective activation of alkanes.

**Keywords:** Alkane Hydrogenolysis, Clusters, Iridium, Single Atoms, Zeolite